

---

This is an electronic reprint of the original article.  
This reprint may differ from the original in pagination and typographic detail.

Gebrehiwot, Silas Z.; Espinosa-Leal, Leonardo; Linderbäck, Paula; Remes, Heikki  
**Experimental investigation and modelling of the nonlinear creep behaviour of additive-manufactured carbon fibre-reinforced polyethylene terephthalate (CF-PET).**

*Published in:*  
Composites Part C: Open Access

*DOI:*  
[10.1016/j.jcomc.2024.100530](https://doi.org/10.1016/j.jcomc.2024.100530)

Published: 01/10/2024

*Document Version*  
Publisher's PDF, also known as Version of record

*Published under the following license:*  
CC BY

*Please cite the original version:*  
Gebrehiwot, S. Z., Espinosa-Leal, L., Linderbäck, P., & Remes, H. (2024). Experimental investigation and modelling of the nonlinear creep behaviour of additive-manufactured carbon fibre-reinforced polyethylene terephthalate (CF-PET). *Composites Part C: Open Access*, 15, Article 100530.  
<https://doi.org/10.1016/j.jcomc.2024.100530>

---

This material is protected by copyright and other intellectual property rights, and duplication or sale of all or part of any of the repository collections is not permitted, except that material may be duplicated by you for your research use or educational purposes in electronic or print form. You must obtain permission for any other use. Electronic or print copies may not be offered, whether for sale or otherwise to anyone who is not an authorised user.



# Experimental investigation and modelling of the nonlinear creep behaviour of additive-manufactured carbon fibre-reinforced polyethylene terephthalate (CF-PET).

Silas Z. Gebrehiwot<sup>a,c,\*</sup>, Leonardo Espinosa-Leal<sup>b</sup>, Paula Linderbäck<sup>c</sup>, Heikki Remes<sup>a</sup>

<sup>a</sup> Department of Mechanical Engineering, Aalto University School of Engineering, Espoo, Finland

<sup>b</sup> Graduate School and Research, Arcada University of Applied Sciences, Helsinki, Finland

<sup>c</sup> School of Engineering, Culture and Wellbeing, Arcada University of Applied Sciences, Helsinki, Finland

## ARTICLE INFO

### Keywords:

Creep strain  
Creep rate  
Nonlinear modelling  
Creep rupture  
Fused filament fabrication

## ABSTRACT

In this paper, the nonlinear creep behaviour of additive-manufactured carbon fibre-reinforced polyethylene terephthalate (CF-PET) is characterised using experimental, theoretical and computational methods. The experimental approach investigates the influence of infill orientations on the creep deformation of the material. For the study, samples at 0°, 45°, and 90° infill orientations are produced with 90% infill density using fused filament fabrication (FFF). The infill orientation parameter highly influences the creep behaviour. Increasing the infill orientation from 0° to 90° monotonically improves the creep resistance of the material, which can be explained by orientation of the fibre-matrix reinforcement towards the uniaxial stresses. Surface examinations of creep-ruptured samples via scanning electron microscopy (SEM) reveal that a combination of matrix failure, fibre pull-out, fibre-matrix debonding, inter-layer debonding, and the presence of voids cause the fractures. Based on the experimental data, the primary and secondary creep responses are modelled theoretically and computationally. The theoretical model is based on the dependence of the material's creep on stress and time parameters at the transient and steady state stages. Combined stress and time functions are used to model the creep of the material. Parallely, two-dimensional (2D) finite element (FE) analyses are made on COMSOL Multiphysics to model the creep computationally. The approach is based on the superposition of Norton's and Garofalo's creep models with predefined time hardening property. The results of the modelling are in good agreement with the experimental findings, showing a maximum of 1.04% for the theoretical, and 2.9% for the computational approaches.

## 1. Introduction

Polymer composites are widely utilised in the construction, maritime, automotive, sports goods and aerospace industries, driven by their desirable properties such as high strength, high stiffness, and lightweight nature [1]. They are synthesised by embedding reinforcement fibres within a base matrix [2]. Based on the constituting materials and method of synthesis, the polymer composites are classified into different categories. These categories include thermosetting with long or woven fibre mat reinforcement; particulate-reinforced thermoplastics, short fibre-reinforced thermoplastic (SFRTs), long fibre impregnated reinforcement; and biopolymers with bio-based filler reinforcements [3,4,

5]. High performance structural composites are largely made from thermosetting composites. However, the precise synthesis process is rather slow and expensive [6]. In addition, the constituting materials and synthesis processes pose greater environmental threats, particularly in large scale production [7,8,9,10]. In response to the challenges, efforts are made to synthesise the composites using bio-based thermosetting resins [7,9]. Regardless, the problems associated with recyclability and end-of-life treatments are still at large [11,12]. On the other hand, promising developments on bio-composites containing bio-degradable matrix and bio-based fillers (fibres) are made to improve environmental sustainability [5,13]. Low carbon-footprints, biocompatibility, recyclability or bio-degradability inspire the emerging

\* Corresponding author.

E-mail address: [silas.gebrehiwot@arcada.fi](mailto:silas.gebrehiwot@arcada.fi) (S.Z. Gebrehiwot).

<sup>a</sup> Corresponding author: Aalto University, department of Mechanical Engineering, Arcada University of Applied Sciences, School of engineering, culture and wellbeing.

demand for sustainable composites. However, higher material development costs, lower mechanical performances, and their manufacturability at a small-scale limit their applicability at a broad range [14].

Nowadays, polymer composites are developed considering their adaptability to different manufacturing methods. In this regard, SFRT composites are versatile for injection moulding, extrusion, and additive manufacturing (AM) methods [15,16,17]. Short fibre reinforcement in polymer composites transfers stresses from the polymer matrix to the fibres, thereby increasing the short and long-term properties of the composite [18]. Consequently, various studies have been reported on polymer matrix composites (PMC) and their applicability in biomedical, automotive, and packaging industries. [19,20,21]. The use of short jute fibre in polypropylene matrix has resulted in a significant improvement of tensile, flexural and impact strength [22]. A short glass fibre-reinforced blend of polyethylene and polyamide-6 polymers was studied by Plamen et al. [23]. They reported 'unusually' high modulus at elevated temperature.

The FFF is widely developing as a manufacturing solution for SFRT products. The low cost, the simplicity of process optimisation, the design freedom, and the versatile applicability make the state-of-the-art manufacturing a viable processing technique. This has attracted the interest of big and medium-scale industries in developing novel 3D printable materials. The ultrafast carbon fibre-reinforced polyethylene terephthalate (CF-PET) by Basf [24], the sustainable polypropylene compound (Beon3D) from LyondellBasell [25], the industrial 3D printable PEEK by Evonik [26] are few to name. Various filaments are currently developed, including bio-based, natural fibre-reinforced, short fibre-reinforced, technical, and blended polymers [27,28,29]. The CF-PET is a recently developed 3D printable filament with good mechanical performance at elevated temperatures. Due to its higher tensile strength, optical clarity, dimensional stability and chemical resistance, PET is commonly used for bottling carbonated drinks and water [30,31,32]. Reinforcing the polymer with short carbon fibre improves its performance at elevated temperatures enhancing key mechanical properties such as stiffness, impact strength, and toughness [29,33]. As a result, versatile applicability of the material at high temperature and stress environments is becoming a possibility. However, rigorous characterisation of the material's performance is required to validate its applicability. Short and long-term creep tests under different load conditions, strain rate and temperature controlled quasi-static tests, and fatigue are some of the experimental approaches that can be used to determine the mechanical properties. In addition, analytical and computational modelling can be utilised to predict the material's response to different loading conditions.

The influences of carbon fibre reinforcement on the mechanical and thermal properties of thermoplastic polymers, including acrylonitrile butadiene styrene (ABS) [34,35], polyamide-PA6 [36], polybutylene terephthalate (PBT) [37], Graphene foam (GF) and polydimethylsiloxane (PDMS) composite [38] are studied. Based on a critical plane damage approach, a theoretical predictive model for fatigue life [39], and computational approach on deformation and failure [40] are proposed for SFRT polymers. The nonlinear viscoelastic behaviour of glass fibre (GF) reinforced polypropylene was studied [41]. The work covers phenomena related to elastic modulus degradation and creep modelling based on the earlier works of Lou and Schapery. Yuan-yuan et al. [42] studied the tensile creep of short CF-reinforced polyetherimide composites. They conduct short-term creep tests using a dynamic mechanical analysis (DMA), examine the influence of the reinforcement on the creep resistance behaviour, and model the creep responses theoretically. The study indicated that the creep resistance increased with the increment in fibre loading. The theoretical approach identified the Findel's power law and the Generalised Maxwell models as suitable to characterise the nonlinear response. On the other hand, the flexural creep of glass fibre-reinforced thermoplastic polymers was modelled using a 4-parameter empirical model [43]. An experimental comparison between glycol-modified PET (PETG) and its short

CF-reinforced counterpart was made by Isaac et al. [44]. Their experimental findings showed a 70.1% increment in tensile modulus and 191.38 % in flexural modulus because of the reinforcement. The effect of recycled CF by weight percentage on the mechanical properties recycled PET is studied using FFF [45]. Their study reported proportional increments of the tensile modulus with a percentage increase in CF content for a 1.75 mm filament diameter.

Modelling the creep behaviour of materials using stress and time functions has been used for metals [46,47,48,49]; however, it is rarely applied to injection moulded or 3D printed polymers. In retrospect, Schapery developed nonlinear creep and proposed a sine hyperbolic stress and a power time functions [50], whereas Findley suggested an empirical power function to characterise the time-dependent deformation [51]. However, as the primary and secondary stages have different creep rates, the models show limitations in characterising the superimposed creep phenomena. Different empirical models were also used to characterise the nonlinear creep behaviour of materials [49]. However, the majority focus on modelling either of the three creep stages (primary, secondary, and tertiary). This has created a lack of versatile models that can present the creep of two or more stages combined. The nonlinear creep behaviour of 3D-printed Polyurethane acrylate (PUA) was studied numerically using a subroutine in Abaqus software [52]. Their study was based on fitting a function on creep compliances obtained experimentally at different stress levels. They used the linear viscoelastic creep compliance relations to develop their nonlinear model. A computational method is used to model the creep of 3D printed PLA, thermoplastic PU (TPU), and polyethylene glycol (PEG) polymer composites [53]. The FE was based on a 3-term Prony series on the Generalised Kelvin model.

Because of its novelty, detailed studies on CF-PET, including experimental investigations on the influences of process parameters on the mechanical properties, failure characterisation, and modelling of deformation at linear and nonlinear regimes, are yet to be reported. In the present work, the nonlinear viscoelastic response of additive-manufactured CF-PET polymer is studied via experimental, theoretical and computational approaches. The main objectives of the paper are to explore the influences of FFF parameters on the creep deformation and rupture phenomena and propose nonlinear creep models theoretically and computationally using semi-empirical approaches. The experimental method is used to investigate the influence of infill orientation on the creep response of the material. Based on the infill orientation parameter, three sample variants ( $0^\circ$ ,  $45^\circ$ ,  $90^\circ$ ) are prepared and tested in uniaxial creep at different stress levels. Ruptured samples are further analysed using SEM to identify the causes of fracture associated with each sample variant. The experimental data are also used to model the nonlinear viscoelastic responses of samples theoretically and computationally. The approaches are based on assigning stress and time functions uniquely associated with the primary and secondary creep responses; hence, they are interrelated. A two-stage regression analysis is made to determine the coefficients of the functions. The computational modelling is made via 2D finite element analyses on COMSOL Multiphysics 6.2.

## 2. Material and methods

### 2.1. Sample preparation

Our samples are designed according to the ISO 527-2, type 1B sample dimensions [54]. And, a commercial short CF-reinforced PET filament from AzureFilm is used to manufacture the samples via FFF technology. The CF-PET filament contains chopped CF with 15% loading by weight. The material is known for its high impact toughness, strength, low water absorption, and maintains its mechanical properties at elevated temperatures [29]. Based on the infill orientation parameter, three sample categories are created at  $0^\circ$ ,  $45^\circ$ , and  $90^\circ$ . In this paper, the term orientation refers to the direction of the infill deposition. This

consideration is different from the conventional definition. In most of the cases, orientation implies the direction of the load with respect to the infill deposition. To clarify the relations, the common terminology and the manner used in this paper to categorise the samples is presented in Fig. 1.

Unlike other commonly used filaments, 3D printing the material requires carefully optimised parameters and safety considerations. This is due to the length scale of chopped reinforcing CF and the fibre-matrix binding chemical used. The nozzle (0.4 mm stainless steel) was set at 290°C, whereas the bed temperature was kept at 90°C during the printing process. For the infill, a line pattern with a 0.5mm top/bottom layer height thickness and a 0.1mm layer height is used. A low infill speed of 50mm/s and a 20% infill fan speed is applied. All samples are manufactured with 90 % infill density. Complying with the safety recommendations, respiratory protection, protective gloves and safety glass were used to avoid hazards associated to the release of fumes while 3D printing at elevated temperatures.

## 2.2. Tensile creep tests

The ISO 899/1:2017 (Plastics. Determination of creep behaviour. Part 1: Tensile creep) standard is followed to test the samples in creep [55]. The tests are defined using a step function where  $\sigma = 0$  at  $t \leq 0$  and  $\sigma = \sigma_0$  at  $t > 0$ .  $\sigma_0$  is the stress amplitude. The step function invokes an infinite strain rate and is practically impossible unless with a smooth stress transition from 0 to  $\sigma_0$ . Therefore, using a 75mm/min test speed ensured attaining the stress amplitude within 1 second. The sample categories are creep tested at different stress ranges. The 0° and 45° samples are tested at 20MPa, 25MPa, 27.5MPa, 30MPa, 32.5MPa and 35MPa, whereas the 90° samples at 20MPa, 25MPa, 30MPa, 35MPa, 40MPa and 45MPa stresses. Each creep test was planned for 3 hours; however, the samples that were tested at higher stresses failed early. The creep tests are made on X350 -20, a high precision digital material testing machine from Testometric Inc. At a 50Hz data acquisition rate, close to 600,000 strain data are obtained for a 3-hour creep test. The creep strain is measured using a high-performance axial extensometer (model 3542) from Epsilon. The summary of the experimental procedure is presented in Table 1.

## 2.3. Scanning electron microscopy (SEM) characterisation

The creep ruptures of the three sample categories are analysed using Zeiss-Sigma VP SEM, a high-quality imaging technology [56]. Due to the samples' non-conductive nature, sputter coating was required. The samples were prepared by depositing 5 nm Gold/Palladium (Au/Pd) for 7 minutes. The fracture surfaces of each sample were investigated from the top.

## 2.4. Modelling the nonlinear creep response

The creep of a material can be studied using a constant stress  $\sigma_0$  in uniaxial tests. Initially, at  $t = 0^+$ , the stress  $\sigma_{t=0^+} = \sigma_0$  causes an instantaneous elastic deformation

$$\varepsilon_o = \frac{\sigma_o}{E}. \quad (1)$$

In eq. (1),  $E$  is the elastic modulus of the material. Eq. (1) holds when the applied stress is well below the yield strength [46]. If the stress is near the yield limit, the instantaneous response of the materials exhibits notable plastic deformation ( $\varepsilon_p$ ) additionally [46]. Therefore, the instantaneous strain  $\varepsilon_{inst}$  becomes

$$\varepsilon_{inst} = \frac{\sigma_o}{E} + \varepsilon_p. \quad (2)$$

As time increases, the material undergoes creep deformation. There are three stages of creep deformation [57]. The classifications are based on the variations of creep strain rate exhibited at each stage. The first one is a primary creep, where the creep strain rate decreases with time. This stage, also referred to as transient creep, emanates from competing material's strain hardening, time hardening or recovery responses [47]. The secondary stage shows approximately constant creep rate, hence regarded as a steady state creep. The stage marks the lowest threshold of the creep rate. It brings nearly linear deformation related to a balance between the hardening (strain hardening) and softening (recovery) processes within the material. For polymeric materials, this stage is regarded as viscous flow, and the deformation is plastic [58]. For semi-crystalline materials, the secondary creep is associated with the motions of dislocations and molecular disentanglements in the amorphous phase [59]. In the case of amorphous materials, the stage is associated with nucleation of voids [60]. At the tertiary stage, a material exhibits an increased creep strain rate, eventually leading to a fracture. The increased creep strain rate is due to the increase in local stresses caused by the specimen's thinning or internal void formation and coalescence [60].

The creep of materials can be modelled by using different combinations of monotonically increasing functions developed through empirical methods. Earlier works by Norton, Soderberg and Bailly showed how different combinations of functions can be used to predict the creep of metallic materials [48]. On the other hand, the nonlinear viscoelastic response can be characterised based on microstructural phenomena. The continuum mechanics hypothesis, superpositions of creep responses on the nonlinear range, and accounting thermodynamic processes are a few of them [51]. The constitutive by Schapery, which is based on irreversible thermodynamic processes states that, under a constant temperature and a uniaxial stress  $\sigma$ , the creep of a nonlinear viscoelastic material is [50]

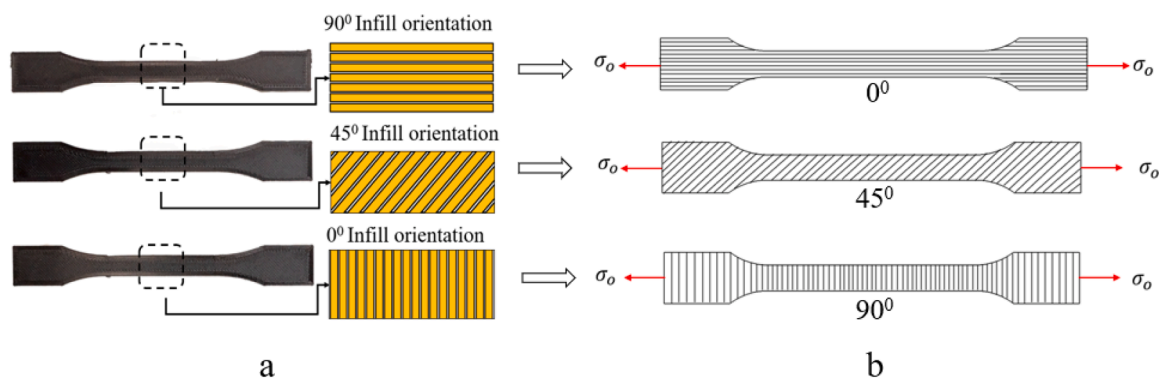


Fig. 1. Additive-manufactured samples; categorised in this paper as a) 0°, 45° and 90° infill orientation, and in b) their relation to the conventional terminology.

**Table 1**

Experimental set up for the tensile creep tests.

Tensile creep experiment							Creep test conditions		
Sample category	Stress amplitude ( $\sigma_o$ )[MPa]						Load function	Max. creep time [s]	Test speed [mm/min]
							0°	20	25
45°	20	25	27.5	30	32.5	35	$\sigma = 0, t \leq 0$		
90°	20	25	30	35	40	45	$\sigma = \sigma_o, t > 0$		

$$\varepsilon(t) = g_0 D_o \sigma(t) + g_1 \int_0^t \Delta D(\varphi - \varphi') \frac{dg_2 \sigma(\tau)}{d\tau} d\tau. \quad (3)$$

In eq. (3),  $g_0, g_1$  and  $g_2$  are stress dependent functions.  $D_o$  and  $\Delta D(\varphi)$  are the time-independent and transient components of the material's compliance respectively. The reduced time  $\varphi$  is further given as

$$\varphi = \varphi(t) = \int_0^t \frac{ds}{a_\sigma[\sigma(s)]}, \text{ and } \varphi' = \varphi(\tau) = \int_0^\tau \frac{ds}{a_\sigma[\sigma(s)]}. \quad (4)$$

In eq. (2),  $a_\sigma$  is a stress-dependent shift factor, whereas  $\tau$  and  $s$  are generic times.

If the creep is caused by a uniaxial constant stress, the time-dependent stress can be given using a Heaviside function  $\sigma(t) = \sigma H(t)$ . Substituting the stress in eq. (3) and evaluating the integration yields

$$\varepsilon(t) = g_0 D_o \sigma + g_1 g_2 \Delta D\left(\frac{t}{a_\sigma}\right) \sigma. \quad (5)$$

As the stress is constant in eq. (5), the first term on the right represents the instantaneous deformation, whereas the second characterises the transient part.

For a uniaxial load, the creep of materials depends on three fundamental parameters. These are the stress, temperature and time [49]. Under a fixed temperature, the time-dependent part of the creep  $\varepsilon_c$  can be given by a combination of stress and time functions. That is,

$$\varepsilon_c = f(\sigma)f(t). \quad (6)$$

The nonlinear creep of materials can be modelled by equating the transient part in eq. (5) with eqn. (6).

$$g_1 g_2 \Delta D\left(\frac{t}{a_\sigma}\right) \sigma = f(\sigma)f(t). \quad (7)$$

This approach was used by Findley [51], but only equating it with a time function, and Schapery [50] with sine hyperbolic stress function. Although it is possible to suggest a stress or a time function in eq. (7), it does not independently represent the two-stage creep deformation of materials. To amend this, the creep stages were separated and modelled using a product of time and stress functions. First, the creep of the material is presented as the sum of the primary and secondary stages.

$$\varepsilon_c = \varepsilon_t + \varepsilon_s. \quad (8)$$

In eq. (8),  $\varepsilon_t$  and  $\varepsilon_s$  are the transient and steady-state creep responses. Based on eqs. (6) and (8), the transient and steady components of the creep can be given using the product of the corresponding stress and time functions. The creep modelling presented in this paper is based on selecting robust functions that can be used to model the transient and steady-state responses with reasonable accuracy. Thus, the primary creep is modelled using power functions of stress and time [46,48,51]. On the other hand, a hyperbolic sine function of stress and a linear function of time are used for the steady state. Substituting the functions in eq. (8), the creep becomes

$$\varepsilon_c = B\sigma^m t^n + \text{Asinh}\left(\frac{\sigma}{\delta}\right)t. \quad (9)$$

In eq. (9),  $A$  and  $\delta$  are stress-independent material constants of the steady state creep, while  $B$  is for the transient. Respectively,  $m$  and  $n$  are the powers of the stress and time functions for the transient creep. Eq. (9) is the equivalent representation for the time-dependent part of the nonlinear creep presented in eq. (3). By including the instantaneous strain, the total strain of the material becomes

$$\varepsilon = \varepsilon_{inst} + \text{Asinh}\left(\frac{\sigma}{\delta}\right)t + B\sigma^m t^n. \quad (10)$$

Eq. (10) gives the instantaneous strain that superimposes the initial elastic and plastic deformations, as well as the creep. However, the focus of this paper is limited to modelling the time-dependent responses, hence the  $\varepsilon_c$  of the different sample categories.

## 2.5. The finite element creep modelling on COMSOL Multiphysics

A 2D FE calculation is made on COMSOL to predict the creep response of the material. COMSOL Multiphysics provides a variety of predefined material models that can be used to study the time-dependent deformation of materials. These include plasticity, viscoelasticity, viscoelasticity, creep, and, nonlinear material models [61]. For the structural analyses, the creep material model is used. In the COMSOL environment, the primary and secondary stages are independently modelled using two subsequent creep models that contribute to the basic linear elastic material model. Our primary creep modelling is closely related to the predefined Norton model [62]. The creep rate at a primary stage is stress and time-dependent; hence

$$\dot{\varepsilon}_{cr} = \lambda \frac{\partial \sigma_e}{\partial \sigma}. \quad (11)$$

In eq. (11),  $\lambda$  is the combined stress and time function,  $Q_e$  is the equivalent stress  $\sigma_e$ , whereas  $\sigma$  is the stress tensor.  $\lambda$  is further given as

$$\lambda = f(\sigma_e) * h(\varepsilon_e, t). \quad (12)$$

The stress function  $f(\sigma_e)$  is modelled as

$$f(\sigma_e) = C \left( \frac{\sigma_e}{\sigma_{ref}} \right)^m. \quad (13)$$

The time hardening of the material is also given as

$$h(\varepsilon_e, t) = n \left( \frac{t + t_{shift}}{t_{ref}} \right)^{n-1}. \quad (14)$$

In eq. (14), the material constant  $C$  is related to the stress function of the proposed theoretical primary creep. That is,  $C = B^* (\sigma_{ref}^m)$ . The  $\sigma_{ref}$  is a reference stress. The stress and time exponents in eqs. (13) and (14) are similar to the theoretical stress function values used to model primary creep. At a specified reference stress  $\sigma_{ref} = 1\text{MPa}$  and reference times  $t_{ref} = 2$  seconds, the constants  $C$ ,  $m$  and  $n$  are determined from the experimental results.

Our secondary stage creep is modelled by adding additional subnode to the primary thereby defining the combined model as

$$\dot{\varepsilon}_{cr} \rightarrow \dot{\varepsilon}_{cr} + \lambda \frac{\partial \sigma_e}{\partial \sigma}. \quad (15)$$

In eq. (15),  $\lambda$  is only a stress function and is defined using Garofalo's

sine hyperbolic as

$$\lambda = D \left[ \sinh \left( \frac{\sigma_e}{\sigma_{ref}} \right) \right]^a \quad (16)$$

In eq. (16) the power of the hyperbolic term,  $a = 1$ , the material constant  $D = A$ , and  $\sigma_{ref} = \delta$ , see eq. (9).

The two-dimensional sample geometry is first imported into the COMSOL Multiphysics graphics window during the computational modelling. Then, the material properties are defined according to the creep models presented above. The boundary settings include constraining the sample geometry at one end and applying the creep load at the other. At the constrained end, the displacement vectors  $\mathbf{u}$  are zero, hence

$$\mathbf{u} = 0. \quad (17)$$

The stress at the other end is defined using a step function  $H(t)$  and applied as a boundary load. That is

$$\sigma = \sigma_o H(t). \quad (18)$$

In eq. (18),  $\sigma_o$  is the stress amplitude, and  $\sigma$  is the applied stress at the boundary. While defining the load using the step function, two continuous derivatives were assigned to avoid convergence errors during the initial time stepping of the solving process. A mapped mesh type with a rectangular element geometry is used for each model. A good mesh statistic was obtained for the selected mesh type. The convergence of the solutions is studied using a parametric sweep on the maximum mesh element size that decreases from 1 mm to 0.1 mm with a 0.1 mm step. Fig. 2 shows the geometry, boundary settings, and mesh details of the specimen domain.

### 3. Results and discussion

#### 3.1. Experimental creep responses

The creep responses of the CF-PET that is additive-manufactured at  $0^\circ$ ,  $45^\circ$  and  $90^\circ$  infill orientations are experimentally studied. The results show that the creep responses strongly depend on the infill orientation parameter, see Figs 3 (a-c).

The creep responses of the sample categories were studied under a wide range of stress levels. The  $90^\circ$  infill orientation samples showed excellent creep performance, whereas poor creep behaviours were observed from the  $0^\circ$  samples. The  $45^\circ$  samples were better than the  $0^\circ$  ones; however, exhibited comparably higher creep deformations than the  $90^\circ$  samples. For example, at  $\sigma = 25\text{MPa}$  and  $t = 3000\text{s}$ , the creep of the  $0^\circ$ ,  $45^\circ$  and  $90^\circ$  samples are 0.00561, 0.00502, and 0.00372, in a corresponding order. The  $0^\circ$  orientation samples exhibited primary and secondary stages without fracture for 20MPa – 27.5MPa stress levels. Creep fracture is detected for 30MPa and above. The sample ruptured at the secondary creep stage when  $\sigma = 30\text{MPa}$ . Raising the stress to 32.5MPa and 35MPa exasperates the creep deformation, leading to a brittle fracture at the early stages of the experiment. The creep performance was comparably better when the samples' infill orientation was at  $45^\circ$ . The samples exhibited secondary stage creep without rupture up

to 32.5MPa stress. A further increment to 35MPa led to a creep fracture within the primary stage. On the other hand, the  $90^\circ$  samples showed the primary and secondary creep stages for the 20MPa – 40MPa stress range. At 45MPa, the sample deformed first in a transient form and swiftly entered the tertiary stage before rupturing at  $t = 2360\text{seconds}$ .

The strain rates of the samples are also evaluated and presented in Figs. 4 (a-c). For all sample variants, the strain rates at lower stress levels swiftly reduce to the minimum values and stay constant at the secondary stage. On the other hand, the transitions among the stages are gradual for the higher stress levels. Generally, the strain rates are very minimal because of the samples' deformations and rupture occurring at small creep strains.

The primary creep is dominated by a hardening process where the creep rate decreases with time and stress. The experimental study showed that this hardening process extended up to the transition into the secondary creep stages. Based on the Figs. 3 (a-c), the creep responses are influenced by the infill orientation parameters. The creep performance monotonically increased with the change of infill orientation from  $0^\circ$  to  $90^\circ$ . This is due to the transition of the infill orientation towards the uniaxial loading. The fractured surface investigation of the samples generally supports this argument. The creep ruptures of the samples are influenced by the fibre and matrix orientations, voids (between layers and within a layer) [63], inter-layer adhesion, fibre-matrix adhesion, and fibre distribution in the matrix. These factors made the polymer composite exhibit different creep fracture phenomena locally.

The creep ruptures were observed at a range of 0.08 – 0.014strain for the three sample categories. The surface examination indicated that the failure mechanism of the samples is associated with the combined effects of fibre pull-out, fibre failure, fibre-matrix debonding, voids (intra and inter-layer), and matrix failure (crazing and microfibril formations) [64]. See the SEM results in Figs. 5 (a-c).

The fracture of the  $0^\circ$  sample is dominated by the failure of the inter-layer matrix. The sample also contains process-related inter-layer and intra-layer voids contributing to the fracture; see subplot 1 of Fig. 5 (a). In addition, fibre-matrix debonding is observed (subplot 2 of Fig. 5 (a)), which results from the perpendicular loading against the infill orientation. Although the infill orientation is perpendicular to the uniaxial creep, there are multiple locations with fibre pull-outs. This indicates that the orientations of the reinforcement fibres cannot only be controlled by the orientation of material deposition (extrusion). Some locations within the matrix domain had river patterns (Fig. 5 (a)) that indicate a brittle fracture. The  $45^\circ$  infill orientation showed different failure mechanisms at the edges and centre of the fracture surfaces. Near the edges, the fracture is dominated by fibre pull-out and intra-layer voids (voids within a layer); see subplots 1 and 2 of Fig. 5 (b). However, the inter-layer matrix failure dominates near the centre (subplot 3 of Fig. 5 (b)). The  $90^\circ$  infill sample failed due to the combined effects of fibre-matrix failure, intra and inter-layer voids, and fibre pull-outs. Longer fibre pull-outs and fibre damages are observed, see subplots 1 & 2 of Fig. 5 (c). In addition, matrix failures with localised fracture planes are common (subplot 3 of Fig. 5 (c)).

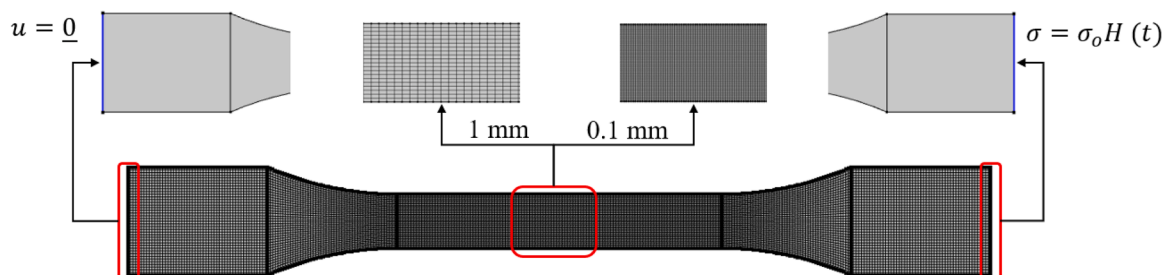


Fig. 2. Geometrical modelling, boundary conditions and meshing for creep analysis on COMSOL Multiphysics.

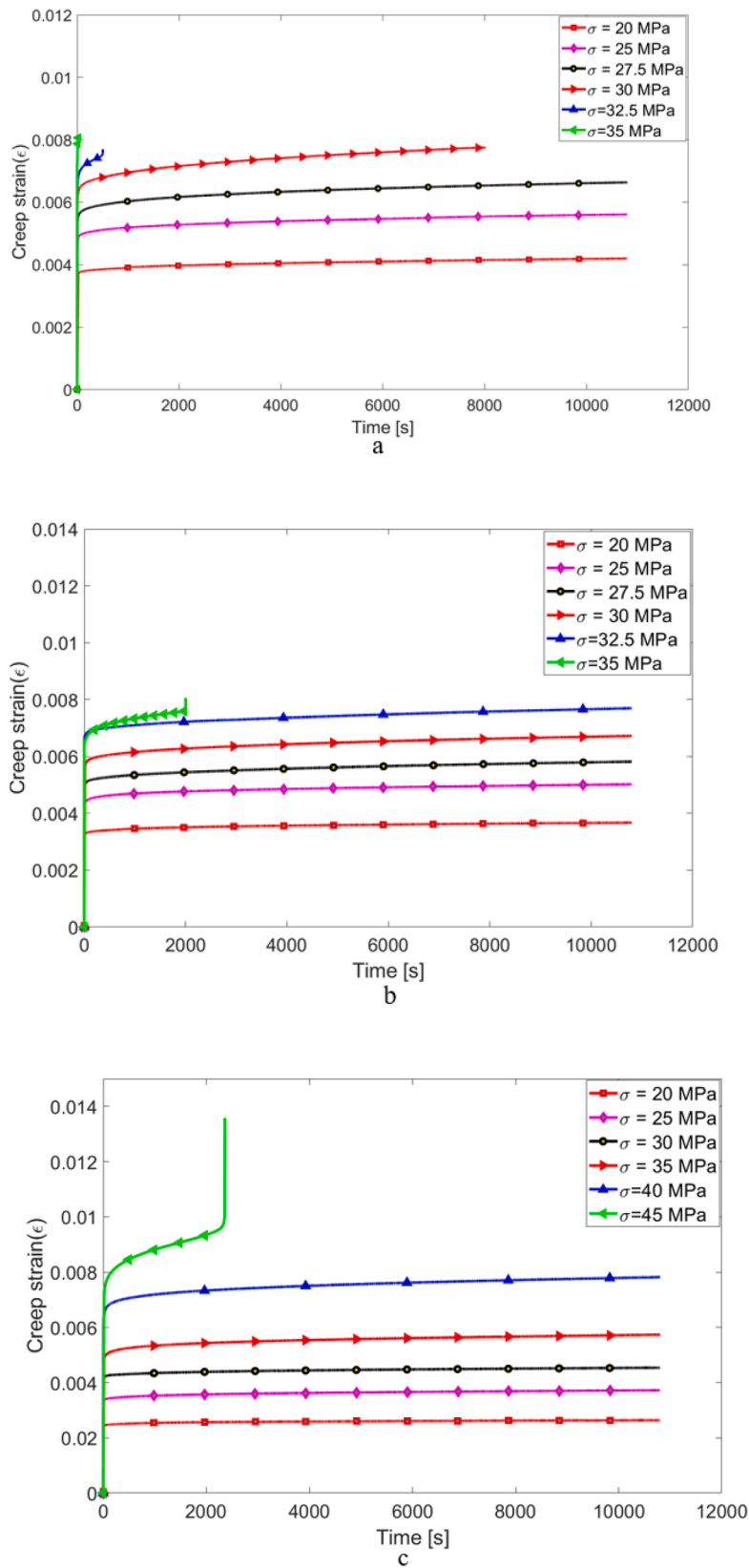


Fig. 3. Experimental creep results: a) 0° infill orientation, b) 45° infill orientation, and c) 90° infill orientation samples.

### 3.2. Determination of material parameters

To model the two stages of the creep, it is essential first to identify the transition from the primary to the secondary creep stage. Hence, the

creep rates of the samples were evaluated to identify the transitions. See Figs. 4 (a-c). After the transitions were determined, the creep stages were modelled separately. The time function of the primary creep has the exponent  $n$ , which is less affected by variations in stress and infill

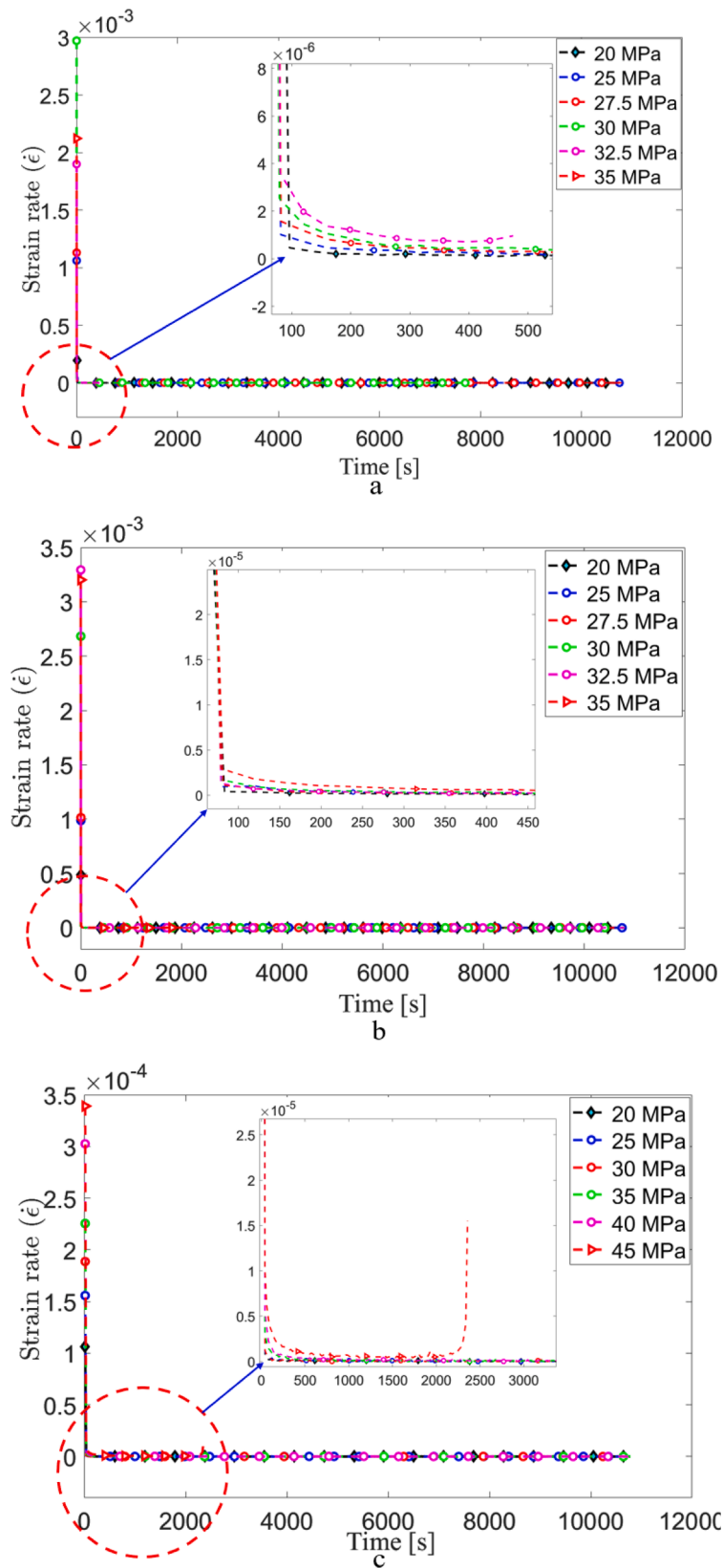
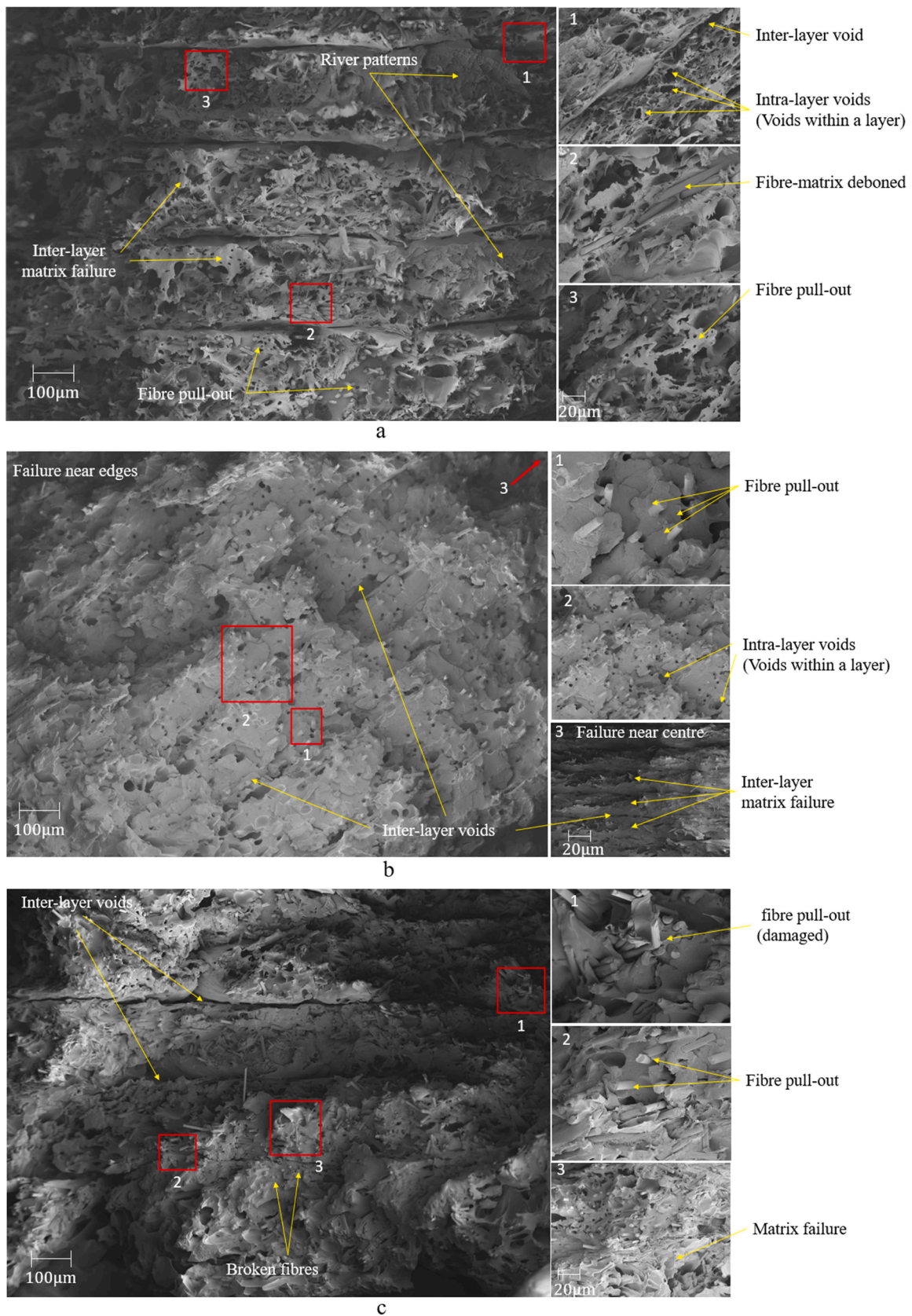


Fig. 4. The strain rates of the a) 0°, b) 45°, and c) 90° infill orientation samples tested at different stress levels.

orientation. For all studied samples,  $n$  varied between 0.2226 and 0.2236. On the other hand, the stress functions for the primary and secondary creep are infill orientation-dependent. A two-step regression analysis is used to determine the material constants related to the stress

functions.

The first step is to use a nonlinear least-square regression on all experimental creep to determine stress-dependent constants associated with the stress functions. The terms in the regression model are related



**Fig. 5.** SEM images of creep ruptured samples a) 0° infill with subplots 1-3 showing different locations with different fracture behaviour b) 45° infill with subplots 1-3 showing different locations with different fracture behaviour c) 90° infill with subplots 1-3 showing different locations with different fracture behaviour.

to eq. (14), however, not robust enough. For each sample category, the curve fitting of the creep data is made using

$$\varepsilon_i = b_i + c_i t + d_i t^n. \quad (19)$$

In eq. (19),  $\varepsilon_i$  is the creep of the material caused by  $\sigma = \sigma_i$ . Comparing eqs. (10) and (19),  $\varepsilon_i = \varepsilon_c$ ,  $b_i = \varepsilon_{insti}$ ,  $c_i = A \sinh\left(\frac{\sigma_i}{\delta}\right)$  and  $d_i = B \sigma_i^m$ .

The second step is to determine the stress-independent material constants ( $B$ ,  $m$ ,  $A$ , and  $\delta$ ). These constants are robust against stress variations and can be determined by plotting  $c_i$  and  $d_i$  with respect to  $\sigma_i$ . The material constants associated with primary creep are determined by imposing a power function relationship between  $d_i$  and  $\sigma_i$ . Fig. 6 shows this relationship for each sample category.

On the other hand, the material constants of the secondary creep are determined by correlating  $c_i$  and  $\sigma_i$  using a sine hyperbolic function, see Fig. 7.

The material constants that are determined from the two-step regression analyses are presented in Table 2. The constants in the stress function depend on infill orientation, while the constant of the time function does not considerably. See Table 2.

### 3.3. The FE analyses

The COMSOL material modelling is also based on the results of the experimental data. However, as indicated in section 2.5, the creep models in COMSOL have material constants related to the theoretical ones. Therefore, the material constants in COMSOL modelling are evaluated using the parameters in Table 2 and assigned to the 2D domain. Fig. 8 presents one of the results of the 2D FE creep (strain component  $\varepsilon_{11}$  in local coordinate system) calculations at  $t = 2.5$ seconds,  $t = 100$ seconds,  $t = 1000$ seconds and  $t = 10800$ seconds.

### 3.4. Comparison of the creep results

Using the material parameters presented in Table 2, the creep responses of the samples are modelled theoretically, and computationally on COMSOL. Figs. 9 (a-c) present the results in comparison to the experimental data.

The theoretically calculated creep responses are all in good agreement with the experimental findings. The stress-independent material parameters are robust against changes in stress; however, they vary slightly with the infill orientation. The differences in the infill reinforcements towards the uniaxial tensile creep cause their variations. The comparisons presented in Figs. 9 also showed a good agreement of

the FE model with experimental results. The errors of the proposed models are evaluated and summarised in Table 3. The theoretical model showed a maximum of 1.04 % for the 45° infill under 32.5 MPa stress, while most of the calculated errors fall below 0.8 %. And, the 2D FE analyses showed a maximum of 2.9 % error for the 0° infill under 20 MPa stress. This indicates that the two-dimensional FE calculation can satisfactorily characterise the creep of the transversally isotropic 3D printed samples. However, the accuracy of the prediction is not as good as the theoretical model. Various reasons can influence the accuracy of predictions, including the spatial dimension considered, the initial time stepping of the load profile, and the boundary conditions. Generally, the error analyses in Table 3 showed that accurate nonlinear creep modelling can be made both theoretically and computationally.

The work characterises the creep deformation of additive-manufactured CF-PET using experimental, theoretical and computational methods. The experimental method focuses on investigating the influences of the infill orientation parameter on the creep performances and rupture mechanisms of the material. The experimental results indicated that the creep deformation of the material improved as the infill orientation changes from 0° to 45° and then to 90°. The maximum creep performance is obtained when the infill is along the loading direction, and the minimum is when the infill is transversal to the loading. The creep performance of the 45° samples is the intermediate. Our previous works on the short-term creep and recovery behaviour [65] and mechanical property optimisation [66] of PLA also revealed similar findings. In addition, studies on the influence of infill orientation on mechanical properties of polymer composites, including the tensile strength and modulus of short carbon fibre-reinforced ABS [67,68], fracture parameter of 3D printed PP [69], flexural strength and modulus of ABS [70], and tensile properties of PLA, ABS and fibre-reinforced nylon [71] suggested similar conclusions. They all identified that samples with 90° orientation (infill along the loading) perform better due to the extrudate reinforcement against the loading.

In this paper, the samples are directly additive manufactured to the net geometry. Hence, it does not imply that the same creep behaviour would be obtained, had the samples were cut to size from large piece of additive manufactured sheet. Additive manufactured components have inherent structural nonuniformities that lead to anisotropy [72,73]. These are associated with the deposition mechanism of the layer structures that usually results in notches, voids, and imperfections at the intra and inter-layer bonding [63]. Cutting samples out of a large structure exasperates the anisotropy by distorting the perimeter (bottom/top layer thickness), and adding post-process phenomena such as, residual stresses due to milling [74], creating heat affected zone (HAZ) within

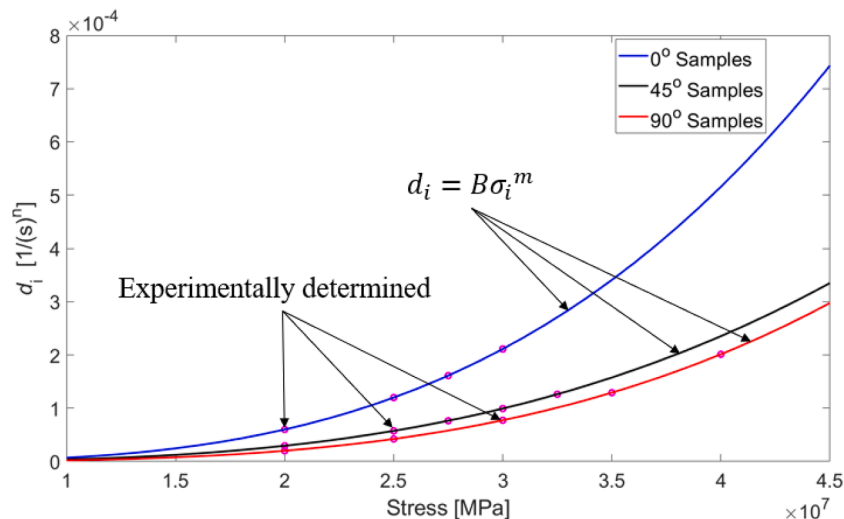


Fig. 6. Curve fitting of  $d_i$  to determine material constants for the primary creep model.

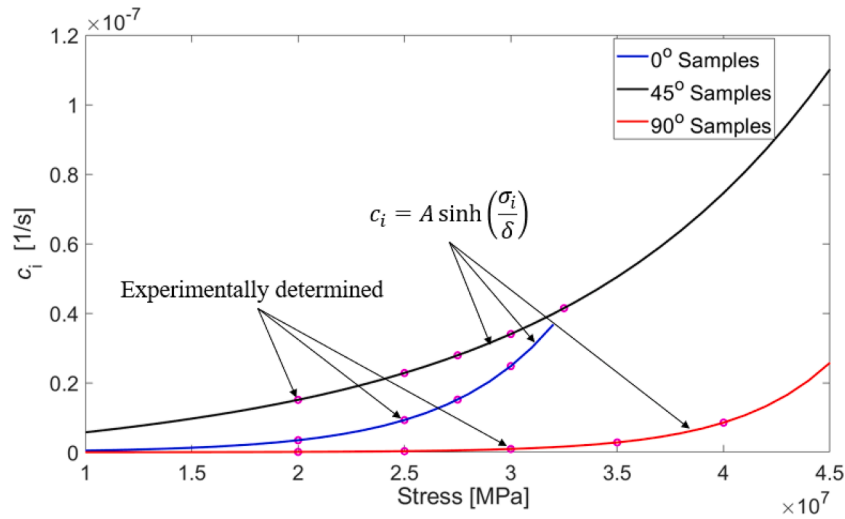


Fig. 7. Curve fitting of  $c_i$  to determine material constants for the secondary creep model.

Table 2

Material constants of the theoretical creep models determined via regression analyses.

Infill orientations	Creep modelling					
	Primary Creep model ( $B\sigma^m t^n$ )			Secondary creep model ( $A \sinh(\frac{\sigma}{\delta}) t$ )		
	Stress function parameters		Time function parameter	Stress function parameters		Time function parameter
	$B$	$m$	$n$	$A$	$\delta$	1
0°	1.328e-27	3.103	0.2226	1.347e-10	5.078e6	-
45°	3.676e-27	3	0.2226	6.662e-9	1.286e7	-
90°	1.161e-29	3.32	0.2236	2.458e-12	4.523e6	-

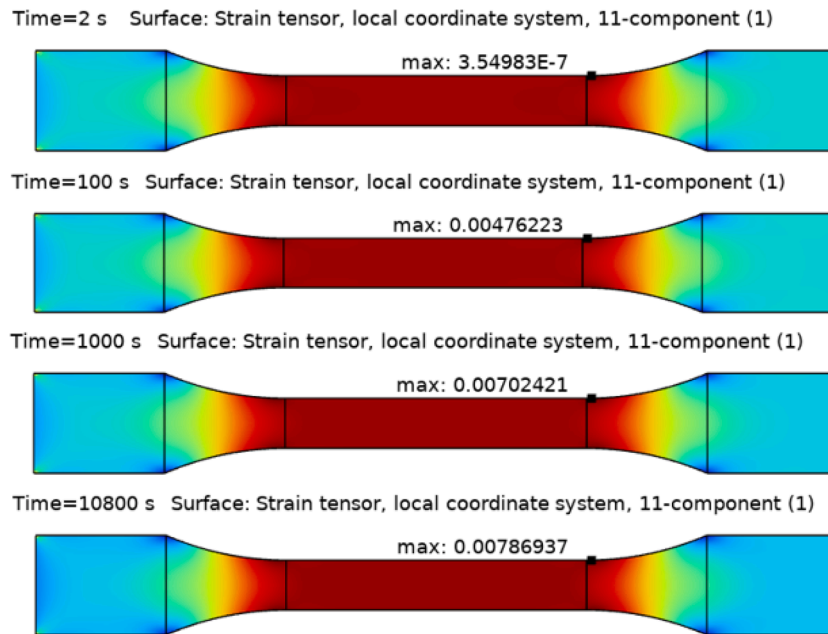


Fig. 8. Surface plots of the creep strain results for the 45° infill orientation sample under 32.5MPa stress.

the sample due to laser cutting, [75,76] or moisture absorption during water jet cutting [74]. Due to these factors, some research works reported that better tensile strength and modulus can be obtained by directly additive manufacturing the specimens than machining [74,75, 77]. On the other hand, cutting the samples out of a large piece removes

the external notches that occur due to the deposition mechanism. This can be considered as an advantage for two reasons: first, it increases the probability of the fracture to be within the gauge length, and second, it improves the ductility property [77]. Whether the samples are directly manufactured or machined out of a sheet, the influences of the infill

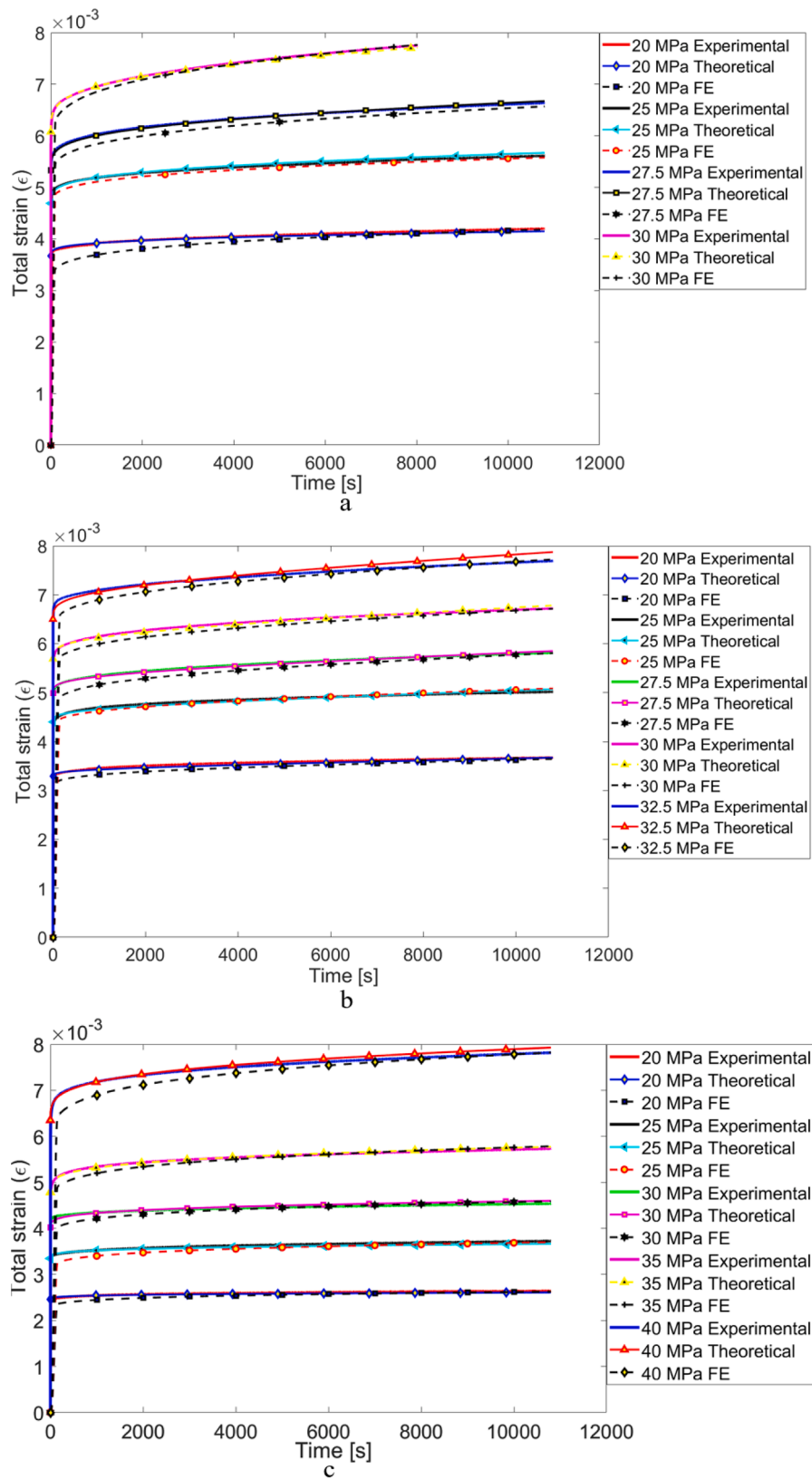


Fig. 9. Experimental creep responses of the material presented in comparison with results of the theoretical and FE approaches for a) 0° samples, b) 45° samples, and c) 90° samples.

**Table 3**  
Mean percentage errors of the theoretical and FE creep models.

Sample category	Creep stress [MPa]	Errors [%]	
		Theoretical model	FE model
0°	20	0.63	2.9
	25	0.61	1.48
	27.5	0.27	2.46
	30	0.32	1.26
45°	20	0.78	2.84
	25	0.53	1.52
	27.5	0.31	2.25
	30	0.41	2.08
	32.5	1.04	2.25
90°	20	0.79	2.67
	25	0.94	2.54
	30	0.82	1.87
	35	0.36	1.73
	40	0.77	2.37

orientations seemed to be similar [74,78]. Good mechanical performances are obtained when the cutting is made longitudinally to infill orientation, while weak performances are the result of cutting made transversally to the infill orientation. However, the authors believe that the influences of specimen cutting direction on long-term mechanical properties, and its comparison to the directly additive-manufactured counterpart could be investigated further.

Analytically, the linear viscoelastic constitutive has been used as a basis for nonlinear viscoelastic modelling. In that regard, few studies are made to characterise the nonlinear viscoelastic behaviours of polymers and polymer composites [79,80,81,82]. In this paper, the theoretical and computational methods focus on characterising the primary and secondary creep phenomena. Uniquely defined stress and time functions are used to predict the material's creep deformation. The coefficients of models are derived from the experimental data via regression analyses. The creep modelling process followed a procedure. First, the transient and steady-state creep stages are separated. Then, appropriate stress and time functions were assigned to each stage. The transient creep was modelled using power functions for the stress and time. Moreover, the steady-state creep was modelled using a sine hyperbolic stress, and a linear time function. The two stages of the creep are presented using a single creep equation, hence superimposed. The material constants  $B$ ,  $m$ ,  $n$ ,  $A$  and  $\delta$  are infill orientation dependent; however, they are closely related. Among these, the powers of the stress and time ( $m$  &  $n$ ) showed consistencies within decimal places, see Table 2. On the other hand, the stress-independent coefficients  $B$ ,  $A$  and  $\delta$  showed notable variations for the different infill geometries. For most materials,  $n$  is generally less than 0.5 [51] while  $m > 1$  or an odd positive integer. Garofalo's creep rupture study in metals reported  $m = 3.64$  for stainless steel at 1300°F and  $m = 4.5$  for aluminium at 500°F [46].

Similarly, COMSOL Multiphysics was used to model the creep response of the material computationally. Slight modifications were made to the COMSOL's predefined creep model. The primary creep is defined using power functions for the stress and the material's time-hardening property, whereas Garofalo's sine hyperbolic stress function is used to model the secondary stage creep. The material constants in the computational model are determined based on their interrelationship with the theoretical counterpart. The proposed models highlight how the material's nonlinear creep is related to stress and time at the primary and secondary creep stages through the material and orientation dependent constants. In particular, within the intermediate to high stress range, the short-term nonlinear creep of the material is generally related to power stress and time functions that explains the hardening at the primary stage, whereas the steady growth at the secondary stage is linearly related with time and nonlinearly with stress. The models adequately reproduced the creep responses of the material. Within the range of stress levels studied, the approaches can be used to model the short-term nonlinear creep of the material. In both approaches, the

models showed good agreement with the experimental findings. The good agreement of the experimental, theoretical and computational methods stems from identifying suitable phenomenological models for a stress and time dependent creep during primary and secondary stages; the use of a wider stress range during the experimental investigation; and the approach (two-step regression process) followed to determine the material constants for the different sample variants.

#### 4. Conclusions

The nonlinear creep behaviour of additive-manufactured CF-reinforced PET is studied using experimental, theoretical and computational methods. The samples are additive-manufactured with 90% infill density and categorised based on three different infill orientation parameters, i.e., 0°, 45° and 90°. The samples are tested in creep at different stress levels, with each creep test lasting up to 3 hours. The experimental creep results are used to compare the sample categories and model their responses theoretically and computationally. The key findings are briefly summarised as follows:

The experimental results revealed a strong dependence of the material's creep performance on the infill orientation parameters. The creep resistance of the material monotonically improved as infill orientation changed from 0° to 45° and then to 90°. Without exhibiting creep rupture, the 0° infill supported a maximum of 27.5MPa stress, while the 45° withstood a 32.5MPa. By comparison, excellent creep performance was obtained from the 90° infill resisting creep rupture up to 40MPa. The successive sample categories (0°, 45°, 90°) showed creep ruptures at 30MPa, 35MPa and 45MPa respectively. The SEM analysis showed that the failures are caused by a variety of localised and non-localised damages. These include matrix failure, fibre, pull-out, fibre-matrix debonding, fibre failure, inter-layer debonding, and voids. Generally, the 90° infill showed good performance which can be explained by the fibre and polymer molecular chains aligning towards the uniaxial stress. On the contrary, the weakest creep performance was obtained from the 0° infill, as the reinforcement did little to support the perpendicular stress.

The theoretical nonlinear creep modelling was based on separating the transient and steady-state contributions through suitably defined stress and time functions. The transient creep was modelled via power stress and time functions, whereas the steady state was based on a sine hyperbolic stress and a linear time function. With almost all calculated errors falling below 1 %, the model's creep predictions were in good agreement with experimental findings. Furthermore, by extending the theoretical model to a computational approach, reasonably acceptable predictions were obtained from 2D-FE calculations. The maximum error of the computational modelling was 2.9%.

#### CRedit authorship contribution statement

**Silas Z. Gebrehiwot:** Conceptualization, Data curation, Formal analysis, Funding acquisition, Investigation, Methodology, Software, Validation, Writing – original draft, Writing – review & editing. **Leonardo Espinosa-Leal:** Funding acquisition, Resources, Supervision, Writing – review & editing. **Paula Linderbäck:** Writing – review & editing. **Heikki Remes:** Supervision, Writing – review & editing.

#### Declaration of competing interest

The authors declare the following financial interests/personal relationships which may be considered as potential competing interests:

Silas Gebrehiwot reports financial support was provided by TUF. If there are other authors, they declare that they have no known competing financial interests or personal relationships that could have appeared to influence the work reported in this paper.

## Acknowledgement

The authors acknowledge Fonden för teknisk undervisning & forskning (TUF) for funding the research project.

## Data availability

Data will be made available on request.

## Reference

- M. F. Ashby, Engineering materials and their properties, in 4th ed. Materials selection in mechanical design, Elsevier Ltd, Butterworth-Heinemann, pp. 31–56, <https://doi.org/10.1016/B978-1-85617-663-7.00003-5>.
- R. Hsissou, R. Seghiri, Z. Benzekri, et al., Polymer composite materials: A comprehensive review, *Composite Structures* 262 (2021), <https://doi.org/10.1016/j.compstruct.2021.113640>.
- S.J. Christian, S.L. Billington, Moisture diffusion and its impact on uniaxial tensile response of biobased composites, *Composites Part B: Engineering* 43 (2012) 2303–2312, <https://doi.org/10.1016/j.compositesb.2011.11.063>.
- R. Payal, Inamuddin, Green Sustainable Process for Chemical and Environmental Engineering and Science, in: T. Altalhi (Ed.), *Green composites: Versatile uses and applications in life*, Elsevier, 2022, p. 165, <https://doi.org/10.1016/B978-0-323-99643-3.00002-4>.
- O. Faruk, A.K. Bledzki, H.P. Fink, M. Sain, Biocomposites reinforced with natural fibers: 2000–2010, *Progress in Polymer Science* 37 (2012) 1552–1596, <https://doi.org/10.1016/j.progpolymsci.2012.04.003>.
- R. J. Crawford, P. J. Martin, General properties of plastics, in 4th ed., *Plastic Engineering*, Elsevier Ltd, Butterworth-Heinemann, pp. 1–57, <https://doi.org/10.1016/C2015-0-00550-0>.
- A.E. Patricia, S.R. Ruben, I. Gandarias, I. Aitziber, G. Koldo, Sustainable Alternatives for the Development of Thermoset Composites with Low Environmental Impact, *Polymers* 15 (2023), <https://doi.org/10.3390/polym15132939>.
- L. Jingkai, et al., Advances in sustainable thermosetting resins: From renewable feedstock to high performance and recyclability, *Progress in Polymer Science* 113 (2021), <https://doi.org/10.1016/j.progpolymsci.2020.101353>.
- L. Jingkai, et al., Recent development on bio-based thermosetting resins, *Journal of polymer science* 59 (2021), <https://doi.org/10.1002/pol.20210328>.
- M. Elisabetta, Tz. Nadka, Recycling of Thermoset Materials and Thermoset-Based Composites: Challenge and Opportunity, *Polymers* 14 (2022), <https://doi.org/10.3390/polym14194153>.
- M. Elisabetta, et al., Recycled (Bio)Plastics and (Bio)Plastic Composites: A Trade Opportunity in a Green Future, *Polymers* 14 (2022), <https://doi.org/10.3390/polym14102038>.
- A.I. Igor, T. Wim, V.B. Bob, Recycling of Polymers: A Review, *ChemSusChem* 7 (2014), <https://doi.org/10.1002/cssc.201300898>.
- J. Jefferson A., H.N. Dhakal, Sustainable biobased composites for advanced applications: recent trends and future opportunities – A critical review, *Composites Part C: Open Access* 7 (2022), <https://doi.org/10.1016/j.jcomc.2021.100220>.
- B.P. Chang, A.K. Mohanty, M. Misra, Studies on durability of sustainable biobased composites: a review, *RSC Adv* 10 (2020), <https://doi.org/10.1039/C9RA09554C>.
- A. Bandar, J. Harri, B. Muneer, A. Abdulhakim, Development of 3D printing short carbon fiber reinforced polypropylene composite filaments, *Journal of Materials Research and Technology* 24 (2023) 16–26, <https://doi.org/10.1016/j.jmrt.2023.02.198>.
- S. Roy et al., Ductile to Brittle Transition of Short Carbon Fiber-Reinforced Polypropylene Composites. (2020), <https://doi.org/10.1155/2020/6714097>.
- J. Proy, et al., Integrating fibers and injection molding process variability in short-natural-fiber-reinforced thermoplastics behavior: A review, *Materials Today Communications* 29 (2021), <https://doi.org/10.1016/j.mtcomm.2021.102785>.
- J. Xiaoyu, G. Qing, Stress-transfer analysis for fibre/matrix interfaces in short-fibre-reinforced composites, *Composites Science and Technology* 61 (2001) 1359–1366, [https://doi.org/10.1016/S0266-3538\(01\)00034-3](https://doi.org/10.1016/S0266-3538(01)00034-3).
- U.S. Darshil, Natural fibre composites: Comprehensive Ashby-type materials selection charts, *Materials & Design* (1980-2015) 62 (2014) 21–31, <https://doi.org/10.1016/j.matdes.2014.05.002>.
- B. Singh, R. Kumar, J.S. Chohan, Polymer matrix composites in 3D printing: A state of art review, *Materials Today: Proceedings* 33 (3) (2020) 1562–1567, <https://doi.org/10.1016/j.matpr.2020.04.335>.
- J. Lijuan, Z. Yinzi, J. Fengnian, Design of short fiber-reinforced thermoplastic composites: A review, *Polymer composites* 43 (8) (2022) 4835–4847, <https://doi.org/10.1002/pc.26817>.
- N. Sultana, et al., Short Jute Fiber Preform Reinforced Polypropylene Thermoplastic Composite: Experimental Investigation and Its Theoretical Stiffness Prediction, *American Chemical Society*, 2023, <https://doi.org/10.1021/acsomega.3c01533>.
- G.M. Plamen, T.D. Ciprian, J.P. Stephen, D.G. Alexandros, Mechanical properties of short fiber reinforced thermoplastic blends, *Polymer* 46 (11) (2005) 3895–3905, <https://doi.org/10.1016/j.polymer.2005.02.091>.
- Basf, Ultrafuse PETCF15. <https://forward-am.com/material-portfolio/ultrafuse-filaments-for-fused-filaments-fabrication-fff/reinforced-filaments/ultrafuse-pet-cf15/>, 2024 (Accessed March 01 2024).
- Lyondellbasell, 3D Printing Meets Sustainability. <https://www.lyondellbasell.com/en/news-events/advancing-possible/3d-printing-meets-sustainability/2024> (Accessed February 25 2024).
- Evonik, Infinity meets reality, INFINAM, 2024. <https://www.infinam.com/en> (Accessed February 15 2024).
- Colorfabb, CIRCULAR MATERIALS DESIGNED BY NATURE. <https://colorfabb.com/sustainability>, 2024 (Accessed January 18 2024).
- Ultimaker, Composite materials for 3D printing. <https://ultimaker.com/materials/composite-materials-for-3d-printing/>, 2024 (Accessed March 02 2024).
- Azurefilm, Carbon Fiber PET filaments. <https://azurefilm.com/product/carbon-fiber-pet-filament/>, 2024 (Accessed January 10 2024).
- B.A. Alshammari, et al., Experimental and Theoretical Analysis of Mechanical Properties of Graphite/Polyethylene Terephthalate Nanocomposites, *Polymers* 14 (2022), <https://doi.org/10.3390/polym14091718>.
- M.J. Tomy, et al., Polyethylene terephthalate (PET) recycling: A review, *Case Studies in Chemical and Environmental Engineering*. 9 (2024), <https://doi.org/10.1016/j.csee.2024.100673>.
- B. Marleine, S. Sabine, M. Rima, Life cycle assessment of two packaging materials for carbonated beverages (polyethylene terephthalate vs. glass): Case study for the lebanese context and importance of the end-of-life scenarios, *Journal of Cleaner Production* 314 (2021), <https://doi.org/10.1016/j.jclepro.2021.128289>.
- L. Qiao, et al., Mechanical Properties, Melting and Crystallization Behaviors, and Morphology of Carbon Nanotubes/Continuous Carbon Fiber Reinforced Polyethylene Terephthalate Composites, *Polymers* 14 (2022), <https://doi.org/10.3390/polym14142892>.
- N. Fuda, C. Weilong, Q. Jingjing, W. Junhua, W. Shiren, Additive manufacturing of carbon fiber reinforced thermoplastic composites using fused deposition modelling, *Composites Part B: Engineering* 80 (2015) 369–378, <https://doi.org/10.1016/j.compositesb.2015.06.013>.
- L.T. Halil, et al., Highly oriented carbon fiber–polymer composites via additive manufacturing, *Composites Science and Technology* 105 (2014) 144–150, <https://doi.org/10.1016/j.compscitech.2014.10.009>.
- Z. Haibin, G. Zhiyong, Z. Dongjie, Z. Guoqun, Enhanced mechanical property of continuous carbon fiber/polyamide thermoplastic composites by combinational treatments of carbon fiber fabric, *Composites Communications* 38 (2023), <https://doi.org/10.1016/j.coco.2023.101508>.
- H. Shyh-shin, Tensile, electrical conductivity and EMI shielding properties of solid and foamed PBT/carbon fiber composites, *Composites Part B: Engineering* 98 (2016) 1–8, <https://doi.org/10.1016/j.compositesb.2016.05.028>.
- Z. Yun-Hong, Z. Ya-Fei, B. Shu-Lin, Y. Xiao-Wen, Carbon fibre/graphene foam/polymer composites with enhanced mechanical and thermal properties, *Composites Part B: Engineering* 94 (2016) 102–108, <https://doi.org/10.1016/j.compositesb.2016.03.056>.
- A. Mohammad, F. Ali, A critical plane approach for multiaxial fatigue life prediction of short fiber reinforced thermoplastic composites, *Composites Part A: Applied Science and Manufacturing* 180 (2024), <https://doi.org/10.1016/j.compositesa.2024.108050>.
- L. Ping, Z. Yucheng, P. Qing-Xiang, S. Viacheslav, Z. Yong-Wei, Simultaneously enhancing the strength and toughness of short fiber reinforced thermoplastic composites by fiber cross-linking, *Composites Science and Technology* 217 (2022), <https://doi.org/10.1016/j.compscitech.2021.109076>.
- B. Margherita, et al., Nonlinear creep behaviour of glass fiber reinforced polypropylene: Impact of aging on stiffness degradation, *Composites Part B: Engineering* 163 (2019) 702–709, <https://doi.org/10.1016/j.compositesb.2019.01.052>.
- Z. Yuan-Yuan, et al., Tensile creep behavior of short-carbon-fiber reinforced polyetherimide composites, *Composites Part B: Engineering* 212 (2021), <https://doi.org/10.1016/j.compositesb.2021.108717>.
- S. Venkata, R. Derrick, M. Gregg, Flexural creep behavior of discontinuous thermoplastic composites: Non-linear viscoelastic modeling and time–temperature–stress superposition, *Composites Part A: Applied Science and Manufacturing* 40 (6–7) (2009) 870–877, <https://doi.org/10.1016/j.compositesa.2009.04.012>.
- D.Vale Ferreira, M. Machado, J. Lino, Additive manufacturing of polyethylene terephthalate glycol /carbon fiber composites: An experimental study from filament to printed parts, *Proceedings of the Institution of Mechanical Engineers, Part L: Journal of Materials: Design and Applications* 233 (2019) 1866–1878, <https://doi.org/10.1177/1464420718795197>.
- K. Amalia, et al., The effect of carbon fiber content on physico-mechanical properties of recycled poly(ethylene terephthalate) composites additively manufactured with fused filament fabrication, *Additive Manufacturing* 60 (2022), <https://doi.org/10.1016/j.addma.2022.103246>.
- I.H. Shames, *Elastic And Inelastic Stress Analysis*, 1st ed., CRC Press, 1997 <https://doi.org/10.1201/b16599>.
- D.P. Miannay, *Structural Integrity Assessment: The Relevant Loading Evaluation. Time-Dependent Fracture Mechanics*, Mechanical Engineering Series, Springer, New York, 2001, pp. 81–140, [https://doi.org/10.1007/978-1-4613-0155-4\\_2](https://doi.org/10.1007/978-1-4613-0155-4_2).
- N. Konstantin, A. Holm, Constitutive model for creep. *Modeling of Creep for Structural Analysis*, Foundations of Engineering Mechanics, Springer, Berlin, Heidelberg, 2007, [https://doi.org/10.1007/978-3-540-70839-1\\_3](https://doi.org/10.1007/978-3-540-70839-1_3).
- R.K. Penny, D.L. Marriott, *Factors affecting strain accumulation. Design for Creep*, 2nd ed., Springer, Dordrecht, 1995 [https://doi.org/10.1007/978-94-011-0561-3\\_2](https://doi.org/10.1007/978-94-011-0561-3_2).
- R.A. Schapery, On the characterization of nonlinear viscoelastic materials, *Polymer Engineering & Science* 9 (4) (1969) 295–310, <https://doi.org/10.1002/pen.760090410>.

- [51] Nonlinear Creep at Constant Stress and Relaxation at Constant Strain, in W. N. Findley, J. S. Lai, & K. Onaran, *Nonlinear Creep at Constant Stress and Relaxation at Constant Strain*, North-Holland Series in Applied Mathematics and Mechanics. 18 (1976), <https://doi.org/10.1016/B978-0-7204-2369-3.50011-4>.
- [52] H. Ruiqi, Z. Xiangyu, C. Yang, Z. Chao, Characterization and prediction of the nonlinear creep behavior of 3D-printed polyurethane acrylate, *Additive Manufacturing* 50 (2022), <https://doi.org/10.1016/j.addma.2021.102583>.
- [53] A. Jayswal, J. Liu, G. Harris, R. Mailen, S. Adanur, Creep behavior of 3D printed polymer composites, *Polymer Engineering & Science* 6 (11) (2023) 3809–3818, <https://doi.org/10.1002/pen.26486>.
- [54] International Organization for Standardization, *Plastics — Determination of tensile properties — Part 1: General principles*, (2019) ISO 527-1:2019.
- [55] International Organization for Standardization, *Plastics- Determination of creep behaviour, Part 1: Tensile creep* (2017). ISO 899-1:2017.
- [56] Zeiss, ZEISS Sigma FE-SEM for High-Quality Imaging & Advanced Analytical Microscopy <https://www.zeiss.com/microscopy/en/products/sem-fib-sem/sem/sigma.html>, (2024) (Accessed January 23 2024).
- [57] G.C. Papanicolaou, & S.P. Zaoutsos, *Viscoelastic constitutive modeling of creep and stress relaxation in polymers and polymer matrix composites*, Composites Science and Engineering, Creep and Fatigue in Polymer Matrix Composites, Woodhead Publishing (2011) 3–47, <https://doi.org/10.1533/9780857090430.1.3>.
- [58] U.W. Gedde, M.S. Hedenqvist, M. Hakkarainen, F. Nilsson, O. Das, *Mechanical Properties*, *Applied Polymer Science* (2021), [https://doi.org/10.1007/978-3-030-68472-3\\_6](https://doi.org/10.1007/978-3-030-68472-3_6).
- [59] A. Dargahi, et al., Nonlinear creep characteristics of extruded Poly (vinylidene fluoride-co-hexafluoropropylene) with high  $\beta$ -phase content under extreme conditions: Design, characterization, and modeling, *Materials & Design* 232 (2023), <https://doi.org/10.1016/j.matdes.2023.112124>.
- [60] A.L. Bowman, et al., Free volume and internal structural evolution during creep in model amorphous polyethylene by Molecular Dynamics simulations, *Polymer* 170 (2019) 85–100, <https://doi.org/10.1016/j.polymer.2019.02.060>.
- [61] COMSOL Multiphysics, *Material models for structural mechanics*. [https://doc.comsol.com/5.6/doc/com.comsol.help.sme/sme Ug\\_modeling.05.057.html](https://doc.comsol.com/5.6/doc/com.comsol.help.sme/sme Ug_modeling.05.057.html), (2024) (Accessed December 17 2023).
- [62] COMSOL Multiphysics, *Creep and viscoplasticity*. [https://doc.comsol.com/6.0/doc/server/#!/com.comsol.help.sme/sme Ug\\_theory.06.33.html](https://doc.comsol.com/6.0/doc/server/#!/com.comsol.help.sme/sme Ug_theory.06.33.html).(2024) (Accessed: January 12 2024).
- [63] T. Yubo, et al., A review on voids of 3D printed parts by fused filament fabrication, *Journal of Materials Research and Technology* 15 (2021) 4860–4879, <https://doi.org/10.1016/j.jmrt.2021.10.108>.
- [64] Y. Denizhan, Z. Ziyang, L. Qingyang, W. Dazhong, Fracture behavior of 3D printed carbon fiber-reinforced polymer composites, *Composites Science and Technology* 208 (2021), <https://doi.org/10.1016/j.compscitech.2021.108741>.
- [65] S. Gebrehiwot, L. Espinosa-Leal, Remes H Andersson, On the Short-Term Creep and Recovery Behaviors of Injection Molded and Additive-Manufactured Tough Poly(lactic Acid) Polymer, *J. of Mater Eng and Perform.* 32 (22) (2023) 10412–10430, <https://doi.org/10.1007/s11665-023-08278-6>.
- [66] S.Z. Gebrehiwot, L. Espinosa-Leal, Remes H Linderbäck, Optimising the mechanical properties of additive-manufactured recycled polylactic acid (rPLA) using single and multi-response analyses methods, *Int J Adv Manuf Technol* 129 (11) (2023) 4909–4924, <https://doi.org/10.1007/s00170-023-12623-3>.
- [67] S. Skhandesh, K. Ozgur, Effect of raster angle on mechanical properties of 3D printed short carbon fiber reinforced acrylonitrile butadiene styrene, *Composites Communications* 32 (2022), <https://doi.org/10.1016/j.coco.2022.101163>.
- [68] M. Somireddy, C. Singh, A. Czekanski, Mechanical behaviour of 3D printed composite parts with short carbon fiber reinforcements, *Engineering Failure Analysis* 107 (2020), <https://doi.org/10.1016/j.engfailanal.2019.104232>.
- [69] M. Lorenzo-Bañuelos, A. Díaz, I. Cuesta, Influence of raster orientation on the determination of fracture properties of polypropylene thin components produced by additive manufacturing, *Theoretical and Applied Fracture Mechanics* (2020) 107, <https://doi.org/10.1016/j.tafmec.2020.102536>.
- [70] C. Ruiqi, B. Liseli, L. James, G. Debbie, Guha M. Senesky, Effects of Part Orientation, Printer Selection, and Infill Density on Mechanical Properties and Production Cost of 3D Printed Flexural Specimens, *Manufacturing Letters* 33 (2022) 549–560, <https://doi.org/10.1016/j.mfglet.2022.07.069>.
- [71] M.J. Martín, J. Auñón, F. Martín, Influence of Infill Pattern on Mechanical Behavior of Polymeric and Composites Specimens Manufactured Using Fused Filament Fabrication Technology, *Polymers* (2021) 13, <https://doi.org/10.3390/polym13172934>.
- [72] John J. Laureto, Joshua M. Pearce, Anisotropic mechanical property variance between ASTM D638-14 type i and type iv fused filament fabricated specimens, *Polymer Testing* 68 (2018) 294–301, <https://doi.org/10.1016/j.polymer.2018.04.029>.
- [73] Angel R. Torrado, David A. Roberson, Failure Analysis and Anisotropy Evaluation of 3D-Printed Tensile Test Specimens of Different Geometries and Print Raster Patterns, *Journal of Failure Analysis and Prevention* 16 (1) (2016), <https://doi.org/10.1007/s11668-016-0067-4>.
- [74] F. Felix, et al., Evaluation of mechanical properties characterization of additively manufactured components, *Progress in Additive Manufacturing* (2024), <https://doi.org/10.1007/s40964-024-00700-2>.
- [75] S.J. Park, Tensile test of additively manufactured specimens with external notch removed via laser cutting in material extrusion, *Polymer Testing* 110 (2022), <https://doi.org/10.1016/j.polymer.2022.107581>.
- [76] K. Ghavidel, A. Shabgard, M. Biglari, Microscopic and mechanical properties of semi-crystalline and amorphous polymeric parts produced by laser cutting, *J. Appl. Polym. Sci.* 133 (44) (2016), <https://doi.org/10.1002/app.44179>.
- [77] Y. Zhang, J.P. Choi, S.K. Moon, Effect of geometry on the mechanical response of additively manufactured polymer, *Polymer Testing* 100 (2021), <https://doi.org/10.1016/j.polymer.2021.107245>.
- [78] L. Yifan, T. Zhenjie, Effect of printing orientation on mechanical properties of SLA 3D-printed photopolymer, *Fatigue & Fracture of Engineering Materials & Structures* 47 (5) (2024) 1531–1545, <https://doi.org/10.1111/ffe.14265>.
- [79] G. Spathis, S. Katsourinis, E. Kontou, Evaluation of fundamental viscoelastic functions by a nonlinear viscoelastic model, *Polymer Engineering & Science* 57 (12) (2017) 1389–1395, <https://doi.org/10.1002/pen.24525>.
- [80] X.R. Xiao, C.C. Hiel, A.H. Cardon, Characterization and modeling of nonlinear viscoelastic response of PEEK resin and PEEK composites, *Composites Engineering* 4 (7) (1994) 681–702, [https://doi.org/10.1016/0961-9526\(94\)90109-0](https://doi.org/10.1016/0961-9526(94)90109-0).
- [81] A. Zacharatos, E. Kontou, Nonlinear viscoelastic modeling of soft polymers, *Journal of Applied Polymer Science* 132 (26) (2015), <https://doi.org/10.1002/app.42141>.
- [82] S.P. Zaoutsos, G.C. Papanicolaou, A.H. Cardon, On the non-linear viscoelastic behaviour of polymer-matrix composites, *Composites Science and Technology* 58 (6) (1998) 883–889, [https://doi.org/10.1016/S0266-3538\(97\)00195-4](https://doi.org/10.1016/S0266-3538(97)00195-4). ISSN 0266-3538.